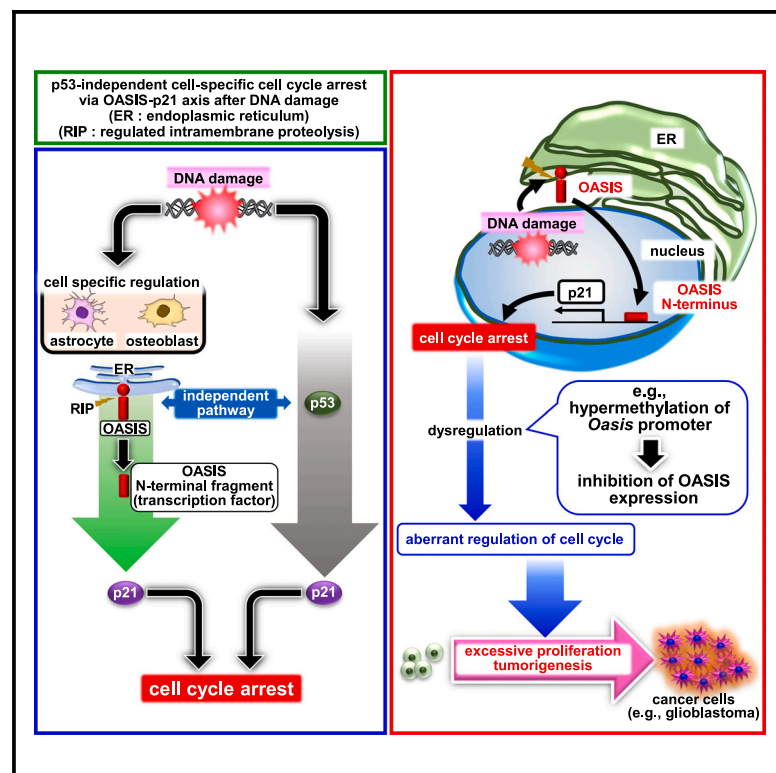


p53-independent tumor suppression by cell-cycle arrest via CREB/ATF transcription factor OASIS

Graphical abstract



Authors

Atsushi Saito, Yasunao Kamikawa, Taichi Ito, ..., Yosuke Matsushita, Toyomasa Katagiri, Kazunori Imaizumi

Correspondence

saitoa@hiroshima-u.ac.jp (A.S.),
imaizumi@hiroshima-u.ac.jp (K.I.)

In brief

Saito et al. demonstrate that OASIS is a critical cell-cycle inhibitor and acts as a functional counterpart to tumor suppressor p53. Recovery of the inhibited OASIS expression in certain types of glioblastomas by their epigenomic engineering treatment suppresses the tumorigenesis, indicating the potential of OASIS as a tumor suppressor.

Highlights

- OASIS arrests the cell cycle of astrocytes at G₂/M phase after DNA damage
- p21-mediated cell-cycle arrest by OASIS or p53 occurs in a cell-specific manner
- Many glioma patients show OASIS downregulation and hypermethylation in its promoter
- Removal of hypermethylation of *Oas1s* promoter inhibits tumorigenesis of glioblastoma



Report

p53-independent tumor suppression by cell-cycle arrest via CREB/ATF transcription factor OASIS

Atsushi Saito,^{1,4,*} Yasunao Kamikawa,¹ Taichi Ito,¹ Koji Matsuhisa,¹ Masayuki Kaneko,² Takumi Okamoto,² Tetsuro Yoshimaru,³ Yosuke Matsushita,³ Toyomasa Katagiri,³ and Kazunori Imaizumi^{1,*}

¹Department of Biochemistry, Institute of Biomedical & Health Sciences, Hiroshima University, Hiroshima 734-8553, Japan

²Department of Pharmacology and Therapeutic Innovation, Nagasaki University Graduate School of Biomedical Sciences, Nagasaki 852-8521, Japan

³Division of Genome Medicine, Institute of Advanced Medical Sciences, Tokushima University, Tokushima 770-8503, Japan

⁴Lead contact

*Correspondence: saitoa@hiroshima-u.ac.jp (A.S.), imaizumi@hiroshima-u.ac.jp (K.I.)

<https://doi.org/10.1016/j.celrep.2023.112479>

SUMMARY

CREB/ATF transcription factor OASIS/CREB3L1 is upregulated in long-term-cultured astrocytes undergoing cell-cycle arrest due to loss of DNA integrity by repeated replication. However, the roles of OASIS in the cell cycle remain unexplored. We find that OASIS arrests the cell cycle at G₂/M phase after DNA damage via direct induction of p21. Cell-cycle arrest by OASIS is dominant in astrocytes and osteoblasts, but not in fibroblasts, which are dependent on p53. In a brain injury model, *Oasis*^{−/−} reactive astrocytes surrounding the lesion core show sustained growth and inhibition of cell-cycle arrest, resulting in prolonged gliosis. We find that some glioma patients exhibit low expression of OASIS due to high methylation of its promoter. Specific removal of this hypermethylation in glioblastomas transplanted into nude mice by epigenomic engineering suppresses the tumorigenesis. These findings suggest OASIS as a critical cell-cycle inhibitor with potential to act as a tumor suppressor.

INTRODUCTION

The cell cycle in eukaryotes is a highly conserved process divided into four sequential phases (G₁, S, G₂, and M).¹ G₁ and G₂/M checkpoints mainly detect the loss of DNA integrity due to internal and external conditions such as DNA damage and incomplete replication, followed by the induction of cell-cycle arrest and repair of the DNA damage.² p53 is a central factor for cell-cycle arrest at these checkpoints. p53 phosphorylated by ataxia telangiectasia mutated (ATM) in response to DNA damage induces the expression of numerous genes related to cell-cycle arrest.^{3,4} Among these genes, p21 is a cyclin-dependent kinase inhibitor whose expression is directly regulated by p53.⁵ Thus, the p53-p21 axis has been accepted to be a unique and critical cascade for cell-cycle arrest. Such arrest of the cell cycle by p53 not only facilitates the repair of DNA damage but also suppresses tumorigenesis.⁶ Loss-of-function mutations of p53 accompanied by a lack of p21-mediated cell-cycle arrest are widely observed in multiple human tumors (more than 50% of all human tumors),⁶ indicating that p53 is a crucial tumor suppressor.

Old astrocyte specifically induced substance (OASIS) is an endoplasmic reticulum (ER)-resident transmembrane transcription factor encoded by the gene *cAMP response element binding protein 3-like 1* (*Creb3l1*). OASIS is cleaved in response to ER stress by regulated intramembrane proteolysis (RIP) through

two different membrane-bound proteases: site-1-protease (S1P) and S2P.^{7,8} Sequential cleavage by S1P and S2P generates N-terminal fragments containing a basic leucine zipper (bZIP)-type DNA binding domain, which act as transcription factors. Our previous studies demonstrated that OASIS is preferentially expressed in specific cells, including astrocytes and osteoblasts, to regulate their differentiation.^{8–10} OASIS is also upregulated at the mRNA level in long-term-cultured astrocytes undergoing cell-cycle arrest by the induction of replicative stress.¹¹ However, the roles of OASIS in the cell cycle have not yet been explored.

RESULTS

OASIS arrests the cell cycle of long-term-cultured and DNA-damaged astrocytes at G₂/M phase

OASIS is an ER-resident transmembrane transcription factor activated by cleavage via RIP (Figure 1A). The generated N-terminal fragments act as transcription factors. We found that full-length OASIS and the cleaved N-terminal fragments were increased during long-term culture of astrocytes with translocation of the OASIS N terminus into the nucleus (Figures 1B and 1C). Repeated replication of long-term-cultured cells induces replicative stress by the loss of DNA integrity due to telomere shortening.¹² Consistent with this, γH2AX, phosphorylated ataxia telangiectasia and Rad3-related (P-ATR), and P-checkpoint kinase 1 (CHK1) (DNA



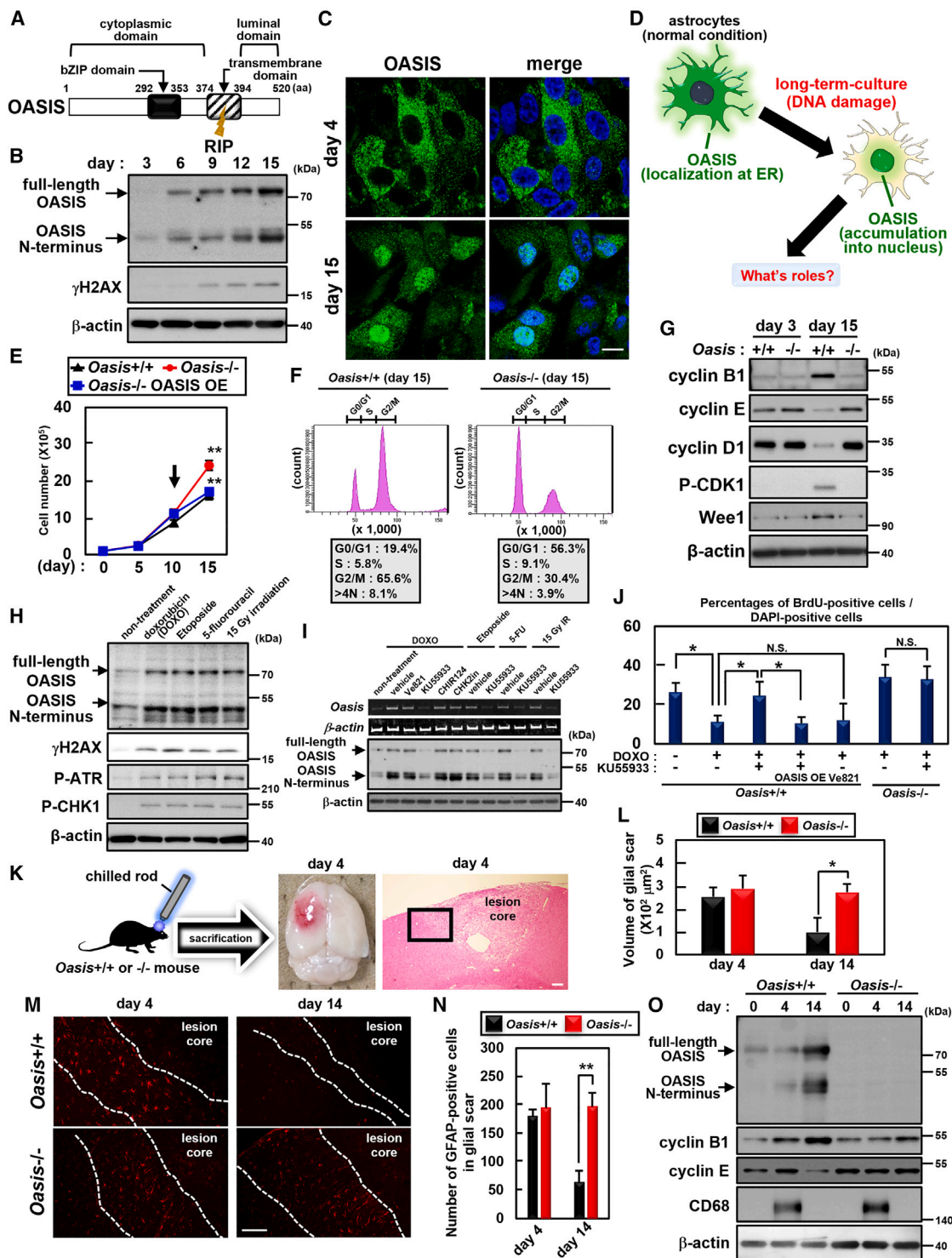


Figure 1. OASIS arrests the cell cycle of astrocytes at G₂/M phase in response to DNA damage

(A) Schema of mouse OASIS. OASIS is cleaved by regulated intramembrane proteolysis (RIP) in response to various cellular stresses, including endoplasmic reticulum (ER) stress. The generated N-terminal fragments containing a basic leucine zipper (bZIP)-type DNA binding domain act as a transcription factor. aa, amino acids.

(B) Western blotting of primary astrocytes.

(C) Immunofluorescence staining of primary astrocytes. The localization of OASIS detected by anti-OASIS N terminus antibody changed from the cytoplasm (day 4) to the nucleus (day 15) during the culture of astrocytes. Right panels show overlap of OASIS (green) and DAPI (blue). Bar: 10 μm.

(legend continued on next page)

damage markers) were upregulated in astrocytes at a late stage of culture (Figures 1B and S1A), indicating that OASIS is cleaved in response to DNA damage to act as a transcription factor (Figure 1D). The number of *Oasis*^{-/-} astrocytes was higher than that of *Oasis*^{+/+} cells at a late stage of culture, with a decreased proportion of cells in G₂/M phase (Figures 1E–1G and S1B–S1E). We also found a higher proportion of >4N cells in long-term-cultured *Oasis*^{+/+} cells. These findings suggest that OASIS arrests the cell cycle at the G₂/M phase in long-term-cultured astrocytes and raise the possibility that *Oasis*^{+/+} astrocytes undergo endoreplication at a late stage of culture.

DNA damage is commonly promoted not only by repeated replication but also by external factors, including anti-cancer drugs and irradiation.¹³ In this study, DNA damage inducers increased the levels of full-length OASIS and its N-terminal fragments, accompanied by translocation of the N-terminal fragments with the upregulation of γ H2AX, P-ATR, and P-CHK1 (Figures 1H and S1F). Although we previously showed that ER stress activates OASIS,¹⁰ the expression of *Spliced form of x-box binding protein 1* (ER stress marker) was hardly detected in doxorubicin (DOXO)-treated and long-term-cultured astrocytes (Figure S1G). Meanwhile, an increased proportion of DOXO-treated astrocytes in G₂/M phase was not observed among *Oasis*^{-/-} cells (Figure S1H). Among inhibitors of each component of the DNA damage response (Figure S1I), treatment with the ATM inhibitor KU55933 only suppressed the induction of OASIS at mRNA and protein levels, which subsequently attenuated the inhibited proliferation of DNA-damaged astrocytes at G₂/M phase (Figures 1I, 1J, S1H, and S1J). The treatment with KU55933 did not affect the number of BrdU-positive *Oasis*^{-/-} astrocytes treated with DNA damage inducer. These results indicate that OASIS arrests the cell cycle at the G₂/M phase downstream of ATM in DNA-damaged astrocytes.

To investigate whether OASIS regulates the cell cycle *in vivo*, we evaluated OASIS expression during gliosis induced by cryoinjury to the brain cortex (Figure 1K).¹¹ Astrocytes transition into reactive astrocytes, featuring cellular hypertrophy, an increased proliferative ability, and upregulation of glial fibrillary acidic protein (GFAP), surrounding the lesion core after damage to the central nervous system.^{14,15} The proliferation of reactive astrocytes is inhibited by the induction of cell-cycle arrest in the late stage of gliosis, which consequently ends the gliosis. In this study, cryoinjury formed a glial scar with the accumulation of abundant reactive astrocytes that strongly expressed GFAP

on day 4 (Figures 1L–1N and S2A). The area was diminished with the upregulation of OASIS and cyclin B1 (G₂/M phase marker) in *Oasis*^{+/+} mice, but not *Oasis*^{-/-} mice, on day 14 (Figures 1L–1O). The expression of cyclin E (G₁ phase marker) was reduced in *Oasis*^{+/+} mice. The level of CD68 (macrophage marker) was almost the same in each stage of *Oasis*^{+/+} and *-/-* mice (Figures 1O and S2B). These findings suggest that OASIS promotes cell-cycle arrest at G₂/M phase in reactive astrocytes to end gliosis, which is consistent with the results obtained using primary astrocytes.

p21-mediated cell-cycle arrest via OASIS or p53 occurs in a cell-specific manner

To explore cell-cycle-related genes directly regulated by the transcription factor OASIS, *Oasis*^{+/+} and *-/-* astrocytes treated with DOXO were subjected to RNA sequencing analysis. Gene Ontology and pathway analyses of genes with an increase or decrease in expression by more than 3-fold upon comparing DOXO-treated *Oasis*^{+/+} and *-/-* astrocytes showed a robust relationship between OASIS and cell cycle regulation (Figures 2A and S3A). A heatmap of cell-cycle-related genes showed that cyclin-dependent kinase inhibitor p21 was only downregulated in *Oasis*^{-/-} astrocytes, despite its upregulation in DNA-damaged *Oasis*^{+/+} astrocytes (Figure S3B). The expression of both p21 and OASIS was increased after the treatment of astrocytes with DOXO (Figure 2B). This elevation was canceled by pretreatment with KU55933 or *Oasis* deficiency. We confirmed the direct induction of p21 by OASIS through binding to a CRE-binding site in the p21 promoter in astrocytes after DNA damage,¹⁶ which induced the G₂/M arrest (Figures S3C–S3G). Although p53 is a main regulator of p21 induction, deficiency or knockdown of OASIS or p53, respectively, did not affect the other's activation in response to DNA damage (Figure 2C), indicating that there is no crosstalk between these pathways.

In contrast to the ubiquitous expression of p53, OASIS is preferentially expressed in certain cell types, including astrocytes and osteoblasts,^{8,10} implying that it is involved in cell-specific regulation of cell-cycle arrest. The numbers of *Oasis*^{-/-} astrocytes and osteoblasts were higher than that of *Oasis*^{+/+} cells at the late stage of culture, with a decrease in the proportion of cells in G₂/M phase (Figures 2D, 2E, and S4A–S4E). The knockdown of p53 did not affect the proliferation. The accelerated proliferation of *Oasis*^{-/-} cells was attenuated by the introduction of p21. The p21 induction in DNA-damaged astrocytes and osteoblasts

(D) Activation process of OASIS in long-term-cultured astrocytes. The downstream pathways and biological events under the control of the activated OASIS during long-term culture are unknown.

(E) Numbers of primary astrocytes (n = 3). Arrow indicates the point when OASIS was introduced. OE, overexpression.

(F) Flow cytometric analysis of primary astrocytes maintained for 15 days.

(G and H) Western blotting of primary astrocytes. Cyclin B1, cyclin E, and cyclin D1 are markers of G₂/M phase, G₁ phase, and G₁/S phase, respectively. P-CDK1 and Wee1 are markers of G₂ phase. P-CDK1, phosphorylated cyclin-dependent kinase 1; P-ATR, phosphorylated ATR; P-CHK1, phosphorylated CHK1.

(I) RT-PCR (top) and western blotting (bottom) of primary astrocytes.

(J) Percentages of BrdU-positive cells among DAPI-positive cells in Figure S1J (n = 6).

(K) Schema for cryoinjury of mouse cerebral cortex. Right panels are images of the cryoinjured brain and H&E staining 4 days after the surgery. Bar: 150 μ m.

(L) Volume of glial scar in Figure S2A (n = 3).

(M) Immunohistochemistry of GFAP in glial scar of the cryoinjured cerebral cortex, indicated by the black box in the right panel of (K). Dotted lines indicate glial scar area. Bar: 150 μ m.

(N) Number of GFAP-positive reactive astrocytes in glial scar in (M) (n = 3).

(O) Western blotting of the cryoinjured side of the cerebral cortex. N.S.: not significant, mean \pm SD, *p < 0.05, **p < 0.01. See also Figures S1 and S2.

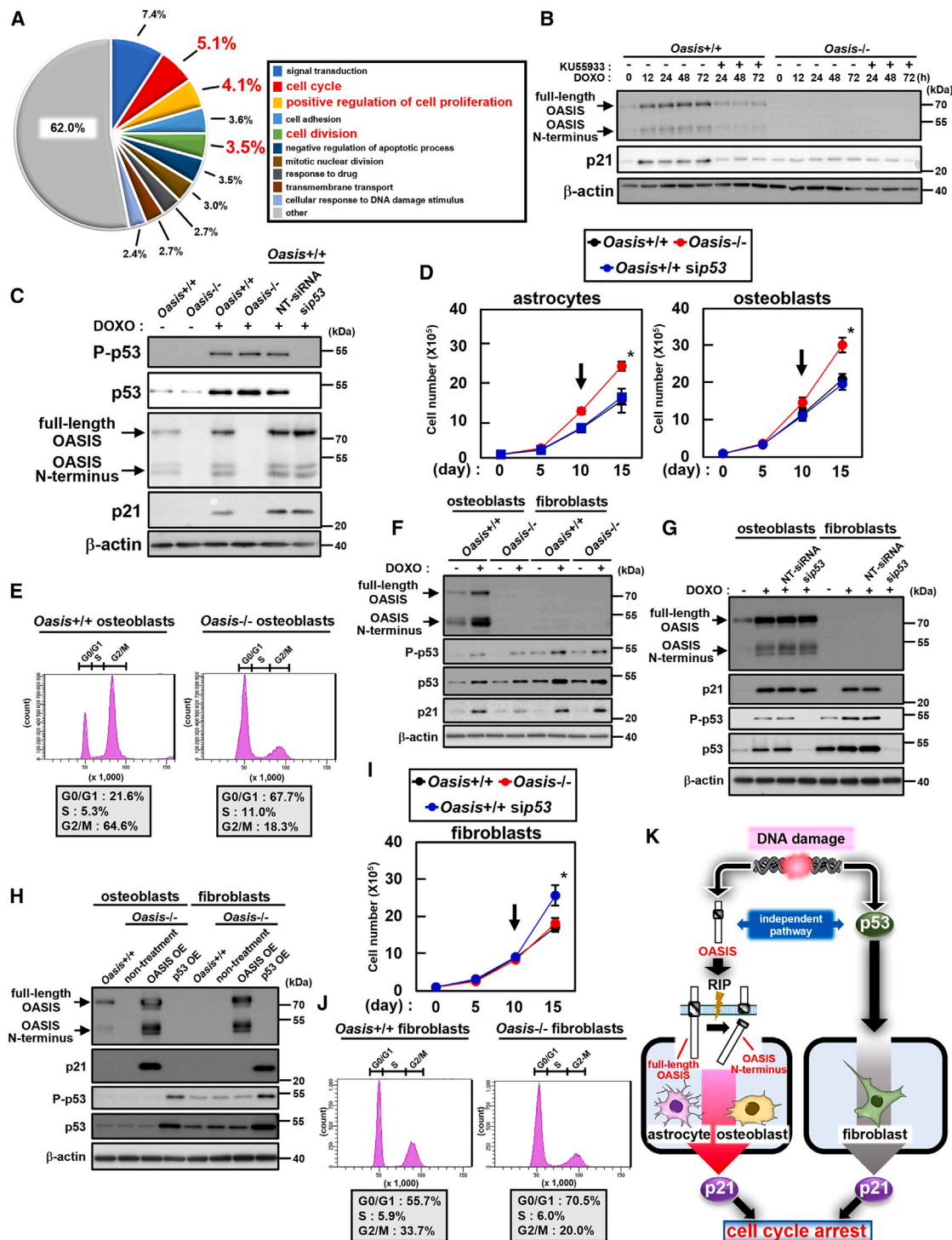


Figure 2. p21-mediated cell-cycle arrest by OASIS or p53 occurs in a cell-specific manner

(A) Gene Ontology analysis of RNA sequencing data (total of 55,488 genes) from primary astrocytes. The second, third, and fifth largest groups are genes related to “cell cycle” (5.1%), “positive regulation of cell proliferation” (4.1%), and “cell division” (3.5%), respectively.
(B and C) Western blotting of primary astrocytes. P-p53, phosphorylated p53; NT-siRNA, non-targeting siRNA.
(D) Numbers of primary astrocytes and osteoblasts (n = 3). Arrows indicate the point when sip53 was introduced.
(E) Flow cytometric analysis of primary osteoblasts maintained for 30 days.
(F–H) Western blotting of primary osteoblasts and fibroblasts.

(legend continued on next page)

depended on OASIS, but not p53 (Figures 2C, 2F–2H, S3C, S3D, S5A, and S5B). OASIS arrested the cell cycle at the G₂/M phase alone via p21 induction in DOXO-treated astrocytes and astrocytes at the late stage of culture, in contrast to the findings for p53 (Figures S3E–S3G and S5C–S5E). Unlike astrocytes and osteoblasts, the p21 upregulation and subsequent inhibition of fibroblast proliferation were predominantly regulated by p53 without an increased population of cells in G₂/M phase (Figures 2F–2J and S4E–S4G). Although a certain amount of p53 was detected in fibroblasts under normal conditions, the expression of p21 was low. It is implied that this much expression of p53 does not upregulate p21 in these cells. Taking these findings together, OASIS arrests the cell cycle at G₂/M phase, and cell-cycle arrest by OASIS or p53 via p21 induction occurs in a cell-specific manner (Figure 2K).

Low expression or loss-of-function mutation of OASIS is linked to glioma development

Loss-of-function mutation of p53 is widely observed in various tumors.⁶ As shown above, OASIS acts as a functional counterpart to p53 to regulate cell-cycle arrest. Although the association between OASIS and tumor was inferred in a previous study,¹⁷ the sample size was small, and no analyses demonstrating the functional relevance were performed. Thus, we carried out an exhaustive analysis to reveal the link between OASIS and tumors using The Cancer Genome Atlas Program (<http://cancergenome.nih.gov/>). As expected, many glioma and glioblastoma patients showed downregulation of OASIS (Figures 3A and S6A). Because one reason for attenuated gene expression is hypermethylation of the gene promoter,¹⁸ we investigated the association between OASIS expression and promoter methylation status. Almost all patients with a highly methylated *Oasis* promoter ($\geq 50\%$) had a low level of OASIS (94.9%). Low expression of p53 was not related to hypermethylation of its promoter (Figure 3B). A large proportion of glioma patients ($\geq 70\%$) were reported to have a mutation in isocitrate dehydrogenase 1 (IDH1).¹⁹ Hence, the involvement of mutation in glioma development has attracted substantial attention. Mutation or low expression of IDH1 attenuates the enzymatic activity of ten-eleven translocation methylcytosine dioxygenase (TET; responsible for DNA demethylation), consequently accelerating extensive DNA methylation.^{20,21} Thus, we examined the involvement of IDH1 dysfunction in the inhibited expression of OASIS due to DNA methylation in its promoter. IDH1-mutated patients with a low OASIS level accounted for 92.8% of patients (Figure 3C) with hypermethylation of its promoter ($\geq 50\%$), which contrasted with the findings for p53 (17.8%). Patients with low IDH1 expression tended to have weak expression of OASIS (98.8%) (Figure 3D). This feature was also observed in patients with other tumors (Figure S7). This tendency was not observed for p53 (23.8%), indicating the potential correlation between deficiency of IDH1 func-

tion and weak expression of OASIS. A large proportion of patients with no detected p53 mutation showed low expression of OASIS (89.1%) (Figure 3E), suggesting a link between OASIS downregulation and glioma development irrespective of p53. p53 mutation is not a necessary and sufficient condition for the onset of glioma (Figure 3F).

We also found that glioblastoma cell lines in the Cancer Cell Line Encyclopedia could be categorized into three patterns in accordance with the expression and methylation status (Figure 3G): (1) a high methylation status and a low expression level (hypermethylation-type, U251MG and LN229 cells with a p53 mutation²²) (Figures 3H, 3I, and S6B–S6E) similar to a certain number of glioma patients, (2) a low methylation status and a high expression level with a loss-of-function mutation as a transcription factor (mutated-type, NP5 and SNU1105 cells with a p53 mutation) (Figures 3I), and (3) others (e.g., U87MG cells). As representative glioblastomas in each category, we selected NP5, U251MG, LN229, and U87MG cells as models for subsequent experiments to investigate the involvement of OASIS in glioblastoma cell proliferation. Among them, upregulation of both OASIS and p21 was only observed in U87MG cells after DNA damage (Figure 3I). The introduction of OASIS, but not the mutated form (R295W) expressed in NP5, into NP5, U251MG, or LN229 cells inhibited their proliferation with the induction of p21 (Figures 3J, 3K, and S8). These results indicate that the OASIS mutation that led to loss of the transcription factor function and weak expression due to hypermethylation of the *Oasis* promoter caused the accelerated proliferation of glioblastoma cell lines. p21 expression was induced in DOXO-treated U87MG cells transfected with si*Oasis* or si*p53* (Figure S9A). p53 knockdown inhibited the induction of p21 in A172 cells (another cell line expressing p53 wild type and quite a low level of OASIS) treated with DOXO (Figure S9B), indicating that p53 mainly induces the expression of p21 in response to DNA damage in A172 cells. Meanwhile, OASIS and p53 may act in a manner complementary to each other to upregulate p21 in several glioblastoma cell lines, such as U87MG cells expressing OASIS. The G₂/M arrest of the three different glioblastoma cell lines (U251MG, U87MG, and A172 cells) was induced via p21 (Figure S10).

Recovery of OASIS expression suppresses tumorigenesis of glioblastoma

Experimentally, U251MG cells expressing full-length OASIS (F9) or its N terminus (N11) exhibited an increase in the proportion of cells in G₂/M phase with the induction of p21 and cellular senescence but not apoptosis (Figures 4A–4C, S11, and S12A–S12D). The higher proportion of >N4 cells and level of cyclin D1 (G₁/S marker) were also observed in F9 cells, compared with those of N11 cells (Figures 4B–4D), implying the possibility of endoreplication by full-length OASIS. Tumorigenesis in nude mice

(I) Numbers of primary fibroblasts ($n = 3$). Arrow indicates the point when si*p53* was introduced.

(J) Flow cytometric analysis of primary fibroblasts maintained for 30 days.

(K) Schema of OASIS- and p53-mediated cell-cycle arrest in response to DNA damage. p21-mediated cell-cycle arrest by OASIS and p53 occurs in a cell-specific manner. OASIS is dominant in upregulating p21 expression, which subsequently arrests the cell cycle at G₂/M phase in astrocytes and osteoblasts. However, p53 preferentially induces p21-mediated inhibition of fibroblast proliferation. These pathways do not have any crosstalk. Mean \pm SD, * $p < 0.05$. See also Figures S3–S5.

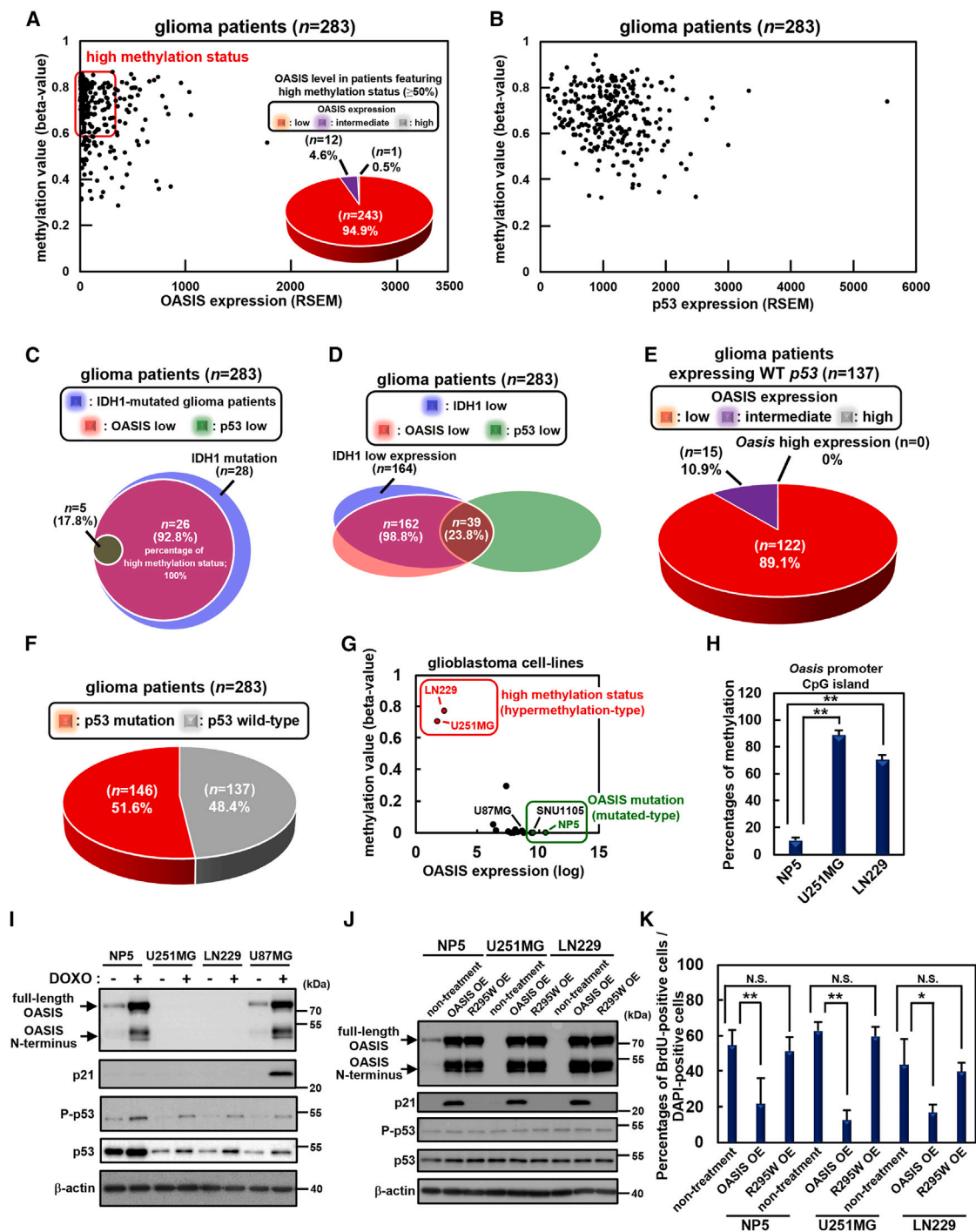


Figure 3. Low expression and loss-of-function mutation of OASIS promote proliferation of glioblastoma

(A) Analysis of OASIS expression and methylation status of the *Oasis* promoter in glioma patients ($n = 283$). Pie chart shows percentages of the categorized expression level of OASIS in patients with hypermethylation ($\geq 50\%$) ($n = 256$). Classifications of low, intermediate, and high show the division of OASIS expression into three equal parts.

(B) Analysis of p53 expression and the methylation status of the *p53* promoter in glioma patients ($n = 283$). The low expression of p53 was not related to hypermethylation of its promoter.

(C and D) Rate of low levels of OASIS or p53 in (C) IDH1-mutated ($n = 28$) and (D) low-IDH1-expressing glioma patients ($n = 164$). Classifications of low, intermediate, and high show the division of IDH1 or p53 expression into three equal parts.

(E) Percentages of each OASIS level in wild-type (WT) p53-expressing glioma patients ($n = 137$).

(legend continued on next page)

transplanted with F9 or N11 was suppressed by p21-mediated cell-cycle arrest (Figures 4E and S12E–S12L). Specific demethylation of the hypermethylated *Oasis* promoter in U251MG cells by CRISPR-based epigenomic engineering using a validated construct²³ expressing a guide RNA (gRNA) targeting the *Oasis* promoter (*Oasis*-gRNA) (Figure S13A) recovered the expression of OASIS and p21, followed by the attenuation of their proliferation (Figures 4F, 4G, and S13B–S13J). The injection of *Oasis*-gRNA-1 into U251MG cells transplanted into nude mice suppressed tumorigenesis via cell-cycle arrest at G₂/M phase due to OASIS and p21 induction and cellular senescence without apoptosis (Figures 4H–4K and S14). Taking these findings together with the existence of a category featuring weak expression of OASIS in tumor patients, OASIS has the potential to act as a critical tumor suppressor.

DISCUSSION

Although OASIS and p53 induce p21-mediated cell-cycle arrest, OASIS specifically arrests the cell cycle at G₂/M phase. As we have shown, OASIS regulates cell-cycle arrest of reactive astrocytes in a glial scar. Astrocytes proliferate as reactive astrocytes in response to brain injury, which subsequently decelerates the cell cycle at the end of gliosis. Astrocytes shift from re-entering the cell cycle to undergoing cell-cycle arrest during these sequential events. Osteoblasts preferentially expressing OASIS also transition from flattened inactive osteoblasts to an active state with exponential proliferation and synthesis of abundant bone matrix during osteogenesis, eventually returning to a quiescent state.^{8,24} Because cells in G₂ phase rapidly enter mitosis compared with G₀ cells, G₂ quiescence is beneficial for specific cells circumstantially switching between re-entry into the cell cycle and cell-cycle arrest.²⁵ Considering that the cell-specific expression of OASIS is distinct from that of p53, G₂/M arrest by OASIS may be necessary for these specific cells to properly switch between cell cycle re-entry and arrest.

In general, a tumor suppressor is defined by several features²⁶: (1) disappearance of the tumor phenotype by its exogenous expression in the tumor, (2) observation of its loss-of-function mutation or weak expression in a large number of tumor patients, and (3) acceleration of tumorigenesis by its deficiency or loss-of-function mutation of both of its alleles. OASIS can thus be defined as a tumor suppressor. Glioma is rare and has an insufficiently definitive classification because of its diverse phenotypes, which has prevented elucidation of the precise molecular mechanisms behind its development. The discovery of a link between OASIS and suppression of glioma development provides new insights for research on glioma and contributes to its classification and understanding of the mechanisms of gli-

oma onset. OASIS is specifically expressed in astrocytes and several other cell types such as osteoblasts. The detailed mechanisms behind the onset of a large number of tumors, including osteosarcoma and glioma, are unknown. The potential of OASIS to suppress tumorigenesis of these tumors thus needs to be assessed, which may lead to novel therapeutic approaches targeting OASIS.

Limitations of the study

One limitation of this study is that we could not uncover the precise mechanisms behind the induction of OASIS by ATM. TET1 is phosphorylated by ATM in response to DNA damage, followed by accelerating the process of DNA demethylation.²⁷ We demonstrated that *Oasis* promoter was demethylated by *Oasis*-gRNA, including the catalytic domain of TET1, implying that the phosphorylation of TET1 by ATM may promote OASIS expression via demethylation of the *Oasis* promoter. Although OASIS-mediated G₂/M arrest leads to end gliosis, the present study could not reveal the detailed differences between cellular senescence by OASIS and G₀/G₁ senescence by p53. Elucidation of the biological purposes of cellular senescence by OASIS is also a significant challenge for future work.

We performed cryoinjury and the following experiments to investigate whether OASIS regulates cell-cycle arrest *in vivo*. Another limitation of this study is that we could not elucidate how the functions of OASIS affect the comprehensive mechanisms of gliosis. Further studies are necessary to uncover all of the roles of OASIS in gliosis.

We demonstrated the roles and responsiveness of OASIS in representative glioblastomas. However, we did not personally authenticate the cell lines that we used by DNA finger printing. Additionally, the analyses of the roles of OASIS in other diverse types of glioblastomas and tumors were insufficient. Further investigations are important to elucidate the involvement of OASIS expression in the characteristics of each glioblastoma and to categorize glioblastoma showing cancer-specific properties dependent on or independent of OASIS activity. These studies may contribute to identifying the specific types of glioblastomas for which OASIS can be considered as a prospective therapeutic target.

We revealed that loss of function of OASIS via its low expression due to high methylation of its promoter may have a greater impact than its mutation on the onset of glioma. Considering previous studies and our own research, none of IDH1, p53, and OASIS is a single determinant of the pathogenesis of glioma. We suggest that OASIS is one of the important factors whose dysfunction has the possibility of promoting glioma development. This complexity is attributable to the diversity of glioma, and further studies are essential to precisely classify glioma based on various loss-of-function molecules.

(F) Percentages of glioma patients (n = 283) expressing mutated p53.

(G) Comparison of OASIS expression and methylation status of the *Oasis* promoter in 16 different glioblastoma cell lines.

(H) Bisulfite sequencing of the *Oasis* promoter in NP5, U251MG, and LN229 cells (n = 5).

(I and J) Western blotting of NP5, U251MG, LN229, and U87MG cells. The levels of p53 and P-p53 were not changed by the induction of OASIS or mutated OASIS (R295W).

(K) Percentages of BrdU-positive cells among DAPI-positive cells in Figures S8D–S8F (n = 6). N.S.: not significant, mean ± SD, *p < 0.05, **p < 0.01. See also Figures S6–S10.

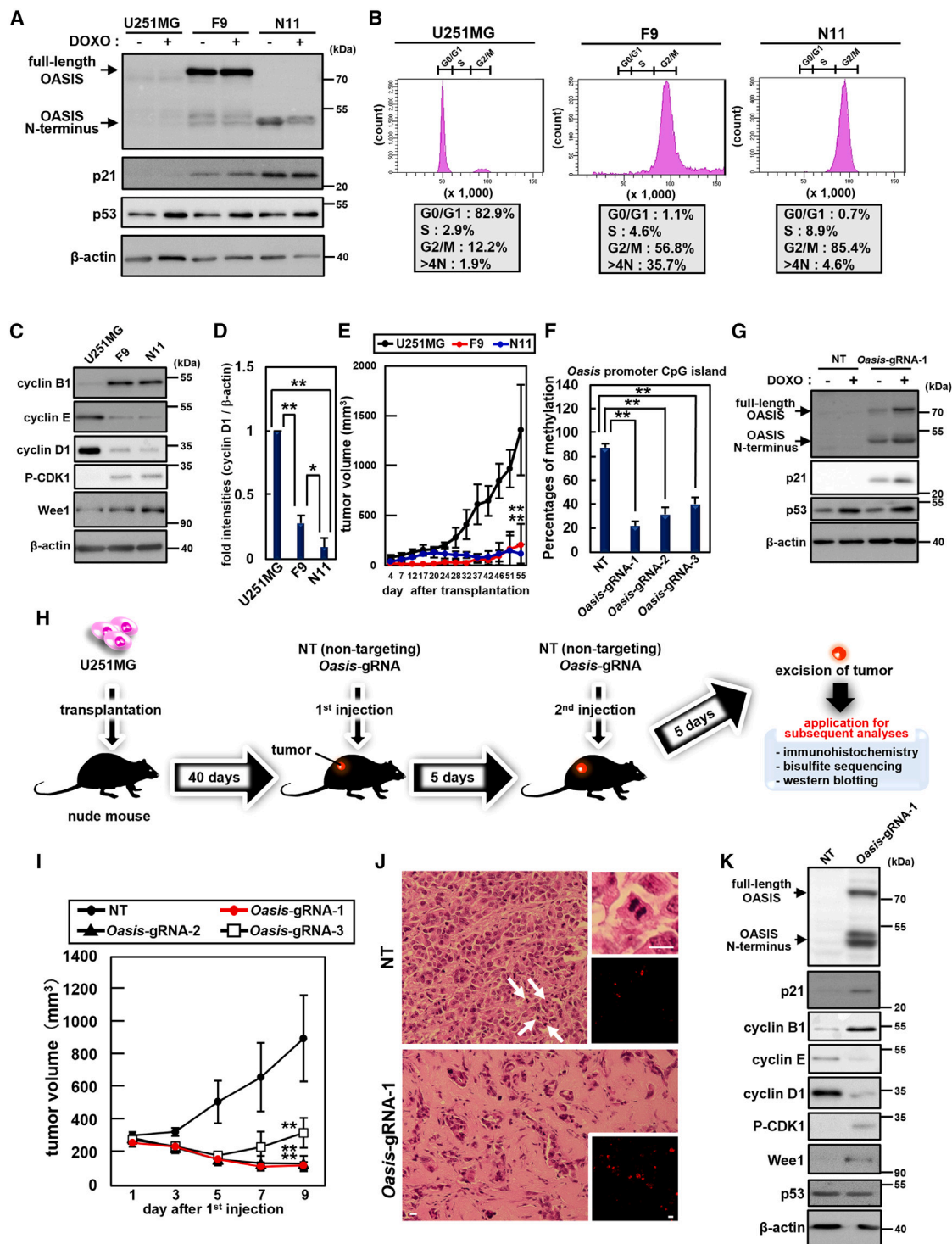


Figure 4. Recovery of OASIS expression suppresses tumorigenesis of glioblastoma

(A) Western blotting of U251MG cells and U251MG cells stably expressing full-length OASIS (F9) or the OASIS N terminus (N11). The level of p53 was not changed in each cell.

(B) Flow cytometric analysis of U251MG, F9, and N11 cells.

(C) Western blotting of U251MG, F9, and N11 cells.

(D) Quantification of relative protein levels of cyclin D1 in (C) (n = 3).

(E) Volume of tumors at the indicated number of days after transplantation (U251MG, n = 5; F9, n = 5; N11, n = 3).

(legend continued on next page)

STAR★METHODS

Detailed methods are provided in the online version of this paper and include the following:

- **KEY RESOURCES TABLE**
- **RESOURCE AVAILABILITY**
 - Lead contact
 - Materials availability
 - Data and code availability
- **EXPERIMENTAL MODEL AND SUBJECT DETAILS**
 - Mice models and maintenance
 - Cell culture and treatments
- **METHODS DETAILS**
 - Plasmids and siRNA
 - Epigenomic engineering
 - RNA isolation and RT-PCR
 - Protein preparation and western blotting
 - Immunofluorescence staining
 - Cell proliferation assay
 - SA- β -gal staining assay
 - TUNEL assay
 - Luciferase assay
 - Bisulfite sequencing
 - Animal surgery
 - Xenograft experiment
 - RNA sequencing
 - Data collection
- **QUANTIFICATION AND STATISTICAL ANALYSIS**

SUPPLEMENTAL INFORMATION

Supplemental information can be found online at <https://doi.org/10.1016/j.celrep.2023.112479>.

ACKNOWLEDGMENTS

This work was partly supported by grants from the Japan Society for the Promotion of Science KAKENHI (JP17H06416, JP20K07573, and JP19K16076), the Sumitomo Electric Industries Group Corporate Social Responsibility Foundation, Takeda Science Foundation, Tsuchiya Foundation, Foundation for Promotion of Cancer Research, Kato Memorial Bioscience Foundation, the Japan Foundation for Pediatric Research Grant No. 20-001, Radiation Effects Association, MSD Life Science Foundation, Public Interest Incorporated Foundation, Princess Takamatsu Cancer Research Fund, Core Research for Organellar Diseases in Hiroshima University (the MEXT Program for Promoting the Enhancement of Research Universities, Japan), the Program of the Network-type Joint Usage/Research Center for Radiation Disaster Medical Science,

Analysis Center of Life Science, the Natural Science Center for Basic Research and Development, Hiroshima University, and Joint Usage and Joint Research Programs, the Institute of Advanced Medical Sciences, Tokushima University. We thank Jin Ye, Ph.D. (the University of Texas, Austin TX, USA), for kindly providing the p21-Luc reporter. We also appreciate the discussions and helpful advice of Masaya Tohyama, Ph.D., and Sadao Shiosaka, Ph.D. Finally, we thank Tom Buckle of Edanz (<https://jp.edanz.com/ac>) for editing a draft of this manuscript.

AUTHOR CONTRIBUTIONS

A.S. and K.I. designed the experiments. A.S., Y.K., T.I., K.M., M.K., and T.O. performed the experiments using cultured cells. T.I. and Y.M. performed the analyses using The Cancer Genome Atlas Program. T.Y., Y.M., and T.K. performed xenograft experiments. A.S. performed histological analyses. A.S. and K.I. wrote the manuscript and supervised the project.

DECLARATION OF INTERESTS

All authors declare no competing financial interests.

Received: October 11, 2022

Revised: February 15, 2023

Accepted: April 20, 2023

Published: May 12, 2023

REFERENCES

1. Baserga, R. (1965). The relationship of the cell cycle to tumor growth and control of cell division: a review. *Cancer Res.* 25, 581–595.
2. Elledge, S.J. (1996). Cell cycle checkpoints: preventing an identity crisis. *Science* 274, 1664–1672. <https://doi.org/10.1126/science.274.5293.1664>.
3. Bates, S., and Vousden, K.H. (1996). p53 in signaling checkpoint arrest or apoptosis. *Curr. Opin. Genet. Dev.* 6, 12–18. [https://doi.org/10.1016/S0959-437X\(96\)90004-0](https://doi.org/10.1016/S0959-437X(96)90004-0).
4. Ismail, I.H., Nyström, S., Nygren, J., and Hammarsten, O. (2005). Activation of ataxia telangiectasia mutated by DNA strand break-inducing agents correlates closely with the number of DNA double strand breaks. *J. Biol. Chem.* 280, 4649–4655. <https://doi.org/10.1074/jbc.M411588200>.
5. el-Deiry, W.S. (1998). Regulation of p53 downstream genes. *Semin. Cancer Biol.* 8, 345–357. <https://doi.org/10.1006/scbi.1998.0097>.
6. Joerger, A.C., and Fersht, A.R. (2007). Structure-function-rescue: the diverse nature of common p53 cancer mutants. *Oncogene* 26, 2226–2242. <https://doi.org/10.1038/sj.onc.1210291>.
7. Murakami, T., Kondo, S., Ogata, M., Kanemoto, S., Saito, A., Wanaka, A., and Imaizumi, K. (2006). Cleavage of the membrane-bound transcription factor OASIS in response to endoplasmic reticulum stress. *J. Neurochem.* 96, 1090–1100. <https://doi.org/10.1111/j.1471-4159.2005.03596.x>.
8. Murakami, T., Saito, A., Hino, S.I., Kondo, S., Kanemoto, S., Chihara, K., Sekiya, H., Tsumagari, K., Ochiai, K., Yoshinaga, K., et al. (2009).

(F) Bisulfite sequencing of the *Oasis* promoter in U251MG cells transfected with non-targeting gRNA construct (NT) or each *Oasis*-gRNA (n = 5). The three *Oasis*-gRNA constructs each express a different gRNA sequence.

(G) Western blotting of U251MG cells transfected with NT or *Oasis*-gRNA-1. The level of p53 was not changed by *Oasis*-gRNA-1.

(H) Schema of *in vivo* injection of *Oasis*-gRNA into a tumor derived from U251MG cells. NT or *Oasis*-gRNA was injected into the U251MG-derived tumor at 40 days after transplantation. These constructs were injected again at 5 days after the first injection. Tumors were excised at 5 days after the second injection, followed by subsequent analyses.

(I) Volume of U251MG cell-derived tumors injected with NT or each *Oasis*-gRNA at the indicated number of days after the first injection (n = 5).

(J) H&E staining of excised tumors in Figure S14A. The population of cells was smaller in the tumor injected with *Oasis*-gRNA-1 with the reduction of mitotic cells than that in the tumor injected with NT. Arrows indicate mitotic cells in the upper right panel. Bottom right panels indicate immunohistochemistry of p21 in excised tumors. Bars: 10 μ m.

(K) Western blotting of excised tumors derived from U251MG cells. Tumors were injected with NT or *Oasis*-gRNA-1. The level of p53 was not changed by the injection of *Oasis*-gRNA-1. Mean \pm SD, *p < 0.05, **p < 0.01. See also Figures S11–S14.

- Signalling mediated by the endoplasmic reticulum stress transducer OASIS is involved in bone formation. *Nat. Cell Biol.* 11, 1205–1211. <https://doi.org/10.1038/ncb1963>.
9. Saito, A., Kanemoto, S., Kawasaki, N., Asada, R., Iwamoto, H., Oki, M., Miyagi, H., Izumi, S., Sanosaka, T., Nakashima, K., and Imaizumi, K. (2012). Unfolded protein response, activated by OASIS family transcription factors, promotes astrocyte differentiation. *Nat. Commun.* 3, 967. <https://doi.org/10.1038/ncomms1971>.
10. Kondo, S., Murakami, T., Tatsumi, K., Ogata, M., Kanemoto, S., Otori, K., Iseki, K., Wanaka, A., and Imaizumi, K. (2005). OASIS, a CREB/ATF-family member, modulates UPR signalling in astrocytes. *Nat. Cell Biol.* 7, 186–194. <https://doi.org/10.1038/ncb1213>.
11. Honma, Y., Kanazawa, K., Mori, T., Tanno, Y., Tojo, M., Kiyosawa, H., Takeda, J., Nikaido, T., Tsukamoto, T., Yokoya, S., and Wanaka, A. (1999). Identification of a novel gene, OASIS, which encodes for a putative CREB/ATF family transcription factor in the long-term cultured astrocytes and gliotic tissue. *Brain Res. Mol. Brain Res.* 69, 93–103. [https://doi.org/10.1016/s0169-328x\(99\)00102-3](https://doi.org/10.1016/s0169-328x(99)00102-3).
12. Olovnikov, A.M. (1996). Telomeres, telomerase, and aging: origin of the theory. *Exp. Gerontol.* 31, 443–448. [https://doi.org/10.1016/0531-5565\(96\)00005-8](https://doi.org/10.1016/0531-5565(96)00005-8).
13. Calcinotto, A., Kohli, J., Zagato, E., Pellegrini, L., Demaria, M., and Altomonte, A. (2019). Cellular senescence: aging, cancer, and injury. *Physiol. Rev.* 99, 1047–1078. <https://doi.org/10.1152/physrev.00020.2018>.
14. Koguchi, K., Nakatsui, Y., Nakayama, K.I., and Sakoda, S. (2002). Modulation of astrocyte proliferation by cyclin-dependent kinase inhibitor p27(Kip1). *Glia* 37, 93–104. <https://doi.org/10.1002/glia.10017>.
15. Mohn, T.C., and Koob, A.O. (2015). Adult astrogenesis and the etiology of cortical neurodegeneration. *J. Exp. Neurosci.* 9, 25–34. <https://doi.org/10.4137/jen.s25520>.
16. Denard, B., Seemann, J., Chen, Q., Gay, A., Huang, H., Chen, Y., and Ye, J. (2011). The membrane-bound transcription factor CREB3L1 is activated in response to virus infection to inhibit proliferation of virus-infected cells. *Cell Host Microbe* 10, 65–74. <https://doi.org/10.1016/j.chom.2011.06.006>.
17. Liu, L.Q., Feng, L.F., Nan, C.R., and Zhao, Z.M. (2018). CREB3L1 and PTN expressions correlate with prognosis of brain glioma patients. *Biosci. Rep.* 38. <https://doi.org/10.1042/bsr20170100>.
18. Herman, J.G. (1999). Hypermethylation of tumor suppressor genes in cancer. *Semin. Cancer Biol.* 9, 359–367. <https://doi.org/10.1006/scbi.1999.0138>.
19. Yan, H., Parsons, D.W., Jin, G., McLendon, R., Rasheed, B.A., Yuan, W., Kos, I., Batnig-Haberle, I., Jones, S., Riggins, G.J., et al. (2009). IDH1 and IDH2 mutations in gliomas. *N. Engl. J. Med.* 360, 765–773. <https://doi.org/10.1056/NEJMoa0808710>.
20. Calvert, A.E., Chalastanis, A., Wu, Y., Hurley, L.A., Kouri, F.M., Bi, Y., Kachman, M., May, J.L., Bartom, E., Hua, Y., et al. (2017). Cancer-associated IDH1 promotes growth and resistance to targeted therapies in the absence of mutation. *Cell Rep.* 19, 1858–1873. <https://doi.org/10.1016/j.celrep.2017.05.014>.
21. Turcan, S., Rohle, D., Goenka, A., Walsh, L.A., Fang, F., Yilmaz, E., Campos, C., Fabius, A.W.M., Lu, C., Ward, P.S., et al. (2012). IDH1 mutation is sufficient to establish the glioma hypermethylator phenotype. *Nature* 483, 479–483. <https://doi.org/10.1038/nature10866>.
22. Van Meir, E.G., Kikuchi, T., Tada, M., Li, H., Diserens, A.C., Wojcik, B.E., Huang, H.J., Friedmann, T., de Tribolet, N., and Cavenee, W.K. (1994). Analysis of the p53 gene and its expression in human glioblastoma cells. *Cancer Res.* 54, 649–652.
23. Morita, S., Noguchi, H., Horii, T., Nakabayashi, K., Kimura, M., Okamura, K., Sakai, A., Nakashima, H., Hata, K., Nakashima, K., and Hatada, I. (2016). Targeted DNA demethylation in vivo using dCas9-peptide repeat and scFv-TET1 catalytic domain fusions. *Nat. Biotechnol.* 34, 1060–1065. <https://doi.org/10.1038/nbt.3658>.
24. Blair, H.C., Sun, L., and Kohanski, R.A. (2007). Balanced regulation of proliferation, growth, differentiation, and degradation in skeletal cells. *Ann. N. Y. Acad. Sci.* 1116, 165–173. <https://doi.org/10.1196/annals.1402.029>.
25. Bedelbaeva, K., Snyder, A., Gourevitch, D., Clark, L., Zhang, X.M., Leferovich, J., Cheverud, J.M., Lieberman, P., and Heber-Katz, E. (2010). Lack of p21 expression links cell cycle control and appendage regeneration in mice. *Proc. Natl. Acad. Sci. USA* 107, 5845–5850. <https://doi.org/10.1073/pnas.1000830107>.
26. Stanbridge, E.J. (1989). The evidence for human tumor suppressor genes. *Princess Takamatsu Symp.* 20, 3–13.
27. Jiang, D., Zhang, Y., Hart, R.P., Chen, J., Herrup, K., and Li, J. (2015). Alteration in 5-hydroxymethylcytosine-mediated epigenetic regulation leads to Purkinje cell vulnerability in ATM deficiency. *Brain* 138, 3520–3536. <https://doi.org/10.1093/brain/awv284>.
28. Cerami, E., Gao, J., Dogrusoz, U., Gross, B.E., Sumer, S.O., Aksoy, B.A., Jacobsen, A., Byrne, C.J., Heuer, M.L., Larsson, E., et al. (2012). The cBio cancer genomics portal: an open platform for exploring multidimensional cancer genomics data. *Cancer Discov.* 2, 401–404. <https://doi.org/10.1158/2159-8290.cd-12-0095>.
29. Gao, J., Aksoy, B.A., Dogrusoz, U., Dresdner, G., Gross, B., Sumer, S.O., Sun, Y., Jacobsen, A., Sinha, R., Larsson, E., et al. (2013). Integrative analysis of complex cancer genomics and clinical profiles using the cBioPortal. *Sci. Signal.* 6, pii1. <https://doi.org/10.1126/scisignal.2004088>.
30. Goldman, M.J., Craft, B., Hastie, M., Repcheck, K., McDade, F., Kamath, A., Banerjee, A., Luo, Y., Rogers, D., Brooks, A.N., et al. (2020). Visualizing and interpreting cancer genomics data via the Xena platform. *Nat. Biotechnol.* 38, 675–678. <https://doi.org/10.1038/s41587-020-0546-8>.
31. Barretina, J., Caponigro, G., Stransky, N., Venkatesan, K., Margolin, A.A., Kim, S., Wilson, C.J., Lehár, J., Kryukov, G.V., Sonkin, D., et al. (2012). The Cancer Cell Line Encyclopedia enables predictive modelling of anticancer drug sensitivity. *Nature* 483, 603–607. <https://doi.org/10.1038/nature11003>.
32. Naito, Y., Hino, K., Bono, H., and Ui-Tei, K. (2015). CRISPRdirect: software for designing CRISPR/Cas guide RNA with reduced off-target sites. *Bioinformatics* 31, 1120–1123. <https://doi.org/10.1093/bioinformatics/btu743>.
33. Kent, W.J., Sugnet, C.W., Furey, T.S., Roskin, K.M., Pringle, T.H., Zahler, A.M., and Haussler, D. (2002). The human genome browser at UCSC. *Genome Res.* 12, 996–1006. <https://doi.org/10.1101/gr.229102>.
34. Huang, D.W., Sherman, B.T., and Lempicki, R.A. (2009). Systematic and integrative analysis of large gene lists using DAVID bioinformatics resources. *Nat. Protoc.* 4, 44–57. <https://doi.org/10.1038/nprot.2008.211>.
35. Huang, D.W., Sherman, B.T., and Lempicki, R.A. (2009). Bioinformatics enrichment tools: paths toward the comprehensive functional analysis of large gene lists. *Nucleic Acids Res.* 37, 1–13. <https://doi.org/10.1093/nar/gkn923>.
36. Wang, Y.E., Kutnetsov, L., Partensky, A., Farid, J., and Quackenbush, J. (2017). WebMeV: a cloud platform for analyzing and visualizing cancer genomic data. *Cancer Res.* 77, e11–e14. <https://doi.org/10.1158/0008-5472.can-17-0802>.
37. Bock, C., Reither, S., Mikeska, T., Paulsen, M., Walter, J., and Lengauer, T. (2005). BiQ Analyzer: visualization and quality control for DNA methylation data from bisulfite sequencing. *Bioinformatics* 21, 4067–4068. <https://doi.org/10.1093/bioinformatics/bti652>.
38. Schindelin, J., Arganda-Carreras, I., Frise, E., Kaynig, V., Longair, M., Pietzsch, T., Preibisch, S., Rueden, C., Saalfeld, S., Schmid, B., et al. (2012). Fiji: an open-source platform for biological-image analysis. *Nat. Methods* 9, 676–682. <https://doi.org/10.1038/nmeth.2019>.
39. Spitzer, M., Wildenhain, J., Rappsilber, J., and Tyers, M. (2014). BoxPlotR: a web tool for generation of box plots. *Nat. Methods* 11, 121–122. <https://doi.org/10.1038/nmeth.2811>.

40. Saito, A., Hino, S.I., Murakami, T., Kanemoto, S., Kondo, S., Saitoh, M., Nishimura, R., Yoneda, T., Furuichi, T., Ikegawa, S., et al. (2009). Regulation of endoplasmic reticulum stress response by a BBF2H7-mediated Sec23a pathway is essential for chondrogenesis. *Nat. Cell Biol.* *11*, 1197–1204. <https://doi.org/10.1038/ncb1962>.
41. Tanenbaum, M.E., Gilbert, L.A., Qi, L.S., Weissman, J.S., and Vale, R.D. (2014). A protein-tagging system for signal amplification in gene expression and fluorescence imaging. *Cell* *159*, 635–646. <https://doi.org/10.1016/j.cell.2014.09.039>.
42. Yoshimaru, T., Komatsu, M., Matsuo, T., Chen, Y.A., Murakami, Y., Mizuguchi, K., Mizohata, E., Inoue, T., Akiyama, M., Yamaguchi, R., et al. (2013). Targeting BIG3-PHB2 interaction to overcome tamoxifen resistance in breast cancer cells. *Nat. Commun.* *4*, 2443. <https://doi.org/10.1038/ncomms3443>.

STAR★METHODS

KEY RESOURCES TABLE

REAGENT or RESOURCE	SOURCE	IDENTIFIER
Antibodies		
Mouse monoclonal anti- β -actin	Sigma-Aldrich	A5441; RRID: AB_476744
Rabbit polyclonal anti-phospho-Histone H2A.X (Ser139/Tyr142)	Cell Signaling Technology	5438; RRID: AB_10707494
Mouse monoclonal anti-p53 (1C12)	Cell Signaling Technology	2524; RRID: AB_331743
Rabbit polyclonal anti-P-p53 (Ser15)	Cell Signaling Technology	9284; RRID: AB_331464
Mouse monoclonal anti-p21 (F-5)	Santa Cruz Biotechnology	sc-6246; RRID: AB_628073
Mouse monoclonal anti-cyclin B1 (GNS1)	Santa Cruz Biotechnology	sc-245; RRID: AB_627338
Mouse monoclonal anti-cyclin E (HE12)	Santa Cruz Biotechnology	sc-247; RRID: AB_627357
Rabbit polyclonal anti-ATR, phospho (Ser428)	Cell Signaling Technology	2853; RRID: AB_2290281
Rabbit monoclonal anti-P-CHK1 Ser345) (133D3)	Cell Signaling Technology	2348; RRID: AB_331212
Rabbit monoclonal anti-cyclin D1 (E3P5S) XP	Cell Signaling Technology	55506; RRID: AB_2827374
Rabbit monoclonal anti-cdc2, phospho (Tyr15) (clone 10A11)	Cell Signaling Technology	4539; RRID: AB_560953
Rabbit polyclonal anti-Wee1	Cell Signaling Technology	4936; RRID: AB_2288509
Rabbit monoclonal anti-CD68 (E3O7V)	Cell Signaling Technology	97778; RRID: AB_2928056
Rabbit monoclonal anti-GFP (D5.1) XP	Cell Signaling Technology	2956; RRID: AB_1196615
Mouse monoclonal anti-BrdU (Bu20a)	Cell Signaling Technology	5292; RRID: AB_10548898
Rabbit polyclonal anti-GFAP	Sigma-Aldrich	G9269; RRID: AB_477035
Mouse monoclonal anti-Ki67 (8D5)	Cell Signaling Technology	9449; RRID: AB_2797703
Mouse monoclonal anti-OASIS N-terminus	Murakami et al. ⁸	N/A
Bacterial and virus strains		
DH5 α	Nippon Gene	310-06231
Chemicals, peptides, and recombinant proteins		
papain	Worthington	LS003124; CAS: 9001-73-4
dispase	Gibco	17105-041; CAS: 42613-33-2
collagenase	Wako	038-22361; CAS: 9001-12-1
puromycin	Wako	160-23151; CAS: 58-58-2
doxorubicin	Wako	040-21521; CAS: 25316-40-9
etoposide	Wako	055-08431; CAS: 33419-42-0
5-fluorouracil	Wako	068-01401; CAS: 51-21-8
Ve821	Adooq Bioscience	A11605; CAS: 1232410-49-9
KU55933	Adooq Bioscience	A10506; CAS: 587871-26-9
CHIR124	Selleck	S2683; CAS: 405168-58-3
CHK2in	Glix Laboratories	GLXC-06231; CAS: 516480-79-8
thapsigargin	Wako	209-17281; CAS: 67526-95-8
Protease Inhibitor Cocktail Set V	Wako	162-26031
5-bromo-2'-deoxyuridine	Sigma-Aldrich	B5002; CAS: 59-14-3
4',6-diamidino-2-phenylindole	Thermo Fisher Scientific	D1306; CAS: 28718-90-3
propidium iodide	Sigma-Aldrich	P4170; CAS: 25535-16-4
staurosporine	Wako	197-10251; CAS: 62996-74-1
DNase I	Nippon Gene	314-08071; CAS: 9003-98-9
GenJet Plus	SignaGen	GL100500
Matrigel	Corning	354234

(Continued on next page)

Continued

REAGENT or RESOURCE	SOURCE	IDENTIFIER
Critical commercial assays		
Senescence β -Galactosidase Staining Kit	Cell Signaling Technology	9860
Cellular Senescence Plate Assay kit SPIDER- β -gal	Dojindo	SG05
DeadEnd Fluorometric TUNEL System	Promega	G3250
Dual-Luciferase Reporter Assay System	Promega	E1910
Methylamp DNA Modification kit	Epigentek	P-1001-1
Deposited data		
RNA-sequencing analysis data	This paper	GEO: GSE229480
Brain Lower-Grade Glioma datasets (TCGA, Firehose Legacy)	The Cancer Genome Atlas Program Cerami et al. ²⁸ Gao et al. ²⁹	http://cancergenome.nih.gov/ cBioportal: https://www.cbioportal.org/
glioblastoma multiforme, prostate cancer, colon cancer, rectal cancer, and sarcoma datasets (TCGA, legacy TCGA)	The Cancer Genome Atlas Program Goldman et al. ³⁰	http://cancergenome.nih.gov/ UCSC Xena Browser: https://xenabrowser.net
gene expression with methylation in glioblastoma cell lines	Cancer Cell Line Encyclopedia Barretina et al. ³¹	https://sites.broadinstitute.org/ccle/
Experimental models: Cell lines		
Human: U251MG cells	JCRB Cell Bank	IFO50288
Human: NP5 cells	JCRB Cell Bank	JCRB1569
Human: LN229 cells	ATCC	CRL-2611
Human: U87MG cells	ATCC	HTB-14
Human: A172 cells	JCRB Cell Bank	JCRB0228
U251MG stably expressing human full-length OASIS (F9)	This paper	N/A
U251MG stably expressing human OASIS N-terminus (N11)	This paper	N/A
Experimental models: Organisms/strains		
Mouse: B6J C57BL/6J	Jackson Laboratory	JAX: 000664
Mouse: B6J C57BL/6J and 129/Sv	Murakami et al. ⁸	N/A
Mouse: BALB/c-nu CAnN.Cg-Foxn1 ^{nu} /CrIcrIj	Jackson Laboratory	JAX: 005512
Oligonucleotides		
non-targeting siRNA	Thermo Fisher Scientific	4390843
siRNA targeting mouse p53	Thermo Fisher Scientific	AM16708; ID: 187426
siRNA targeting human p53	Thermo Fisher Scientific	4390824; ID: s607
siRNA targeting mouse p21	Thermo Fisher Scientific	4390771; ID: s63812
siRNA targeting human p21	Thermo Fisher Scientific	4390824; ID: s415
siRNA targeting human OASIS	Thermo Fisher Scientific	4392420; ID: s40546
Primer: OASIS Forward: GAACATGGAGGACTTCTCCAATG	This paper	N/A
Primer: OASIS Reverse: CGGGCTCTGCTCCTGCTTCAC	This paper	N/A
Primer: XBP1 Forward: ACACGCTTGGAATGGACAC	This paper	N/A
Primer: XBP1 Reverse: CCATGGGAAGATGTTCTGGG	This paper	N/A
Primer: β -actin Forward: TCCTCCCTGGAGAAGAGCTA	This paper	N/A
Primer: β -actin Reverse: TCCTGCTTGCTGATCCACAT	This paper	N/A
Primer: OASIS CpG island Forward: GTTGTTTTAAGTTTTATTTTGAG	This paper	N/A

(Continued on next page)

Continued

REAGENT or RESOURCE	SOURCE	IDENTIFIER
Primer: OASIS CpG island Reverse: TAACACCCTAAAATTTCTAAACC	This paper	N/A
Primer: p53 CpG island Forward: TAGAGTTAAAGAAATTTATTTGTG	This paper	N/A
Primer: p53 CpG island Reverse: CTAAAACCTAAAAATAAATAC	This paper	N/A
Non-targeting gRNA sequence: GTACGTCGGTATAACTCCTC	This paper	N/A
gRNA inserted in <i>Oasis</i> -gRNA-1 construct: CCTGAAGCCCTCAGCCCCAACCC	This paper	N/A
gRNA inserted in <i>Oasis</i> -gRNA-2 construct: TGGAACCCCTCCCGGCCGACAGG	This paper	N/A
gRNA inserted in <i>Oasis</i> -gRNA-3 construct: ATAGGCTGGATCTCCGCTGGGGG	This paper	N/A

Recombinant DNA

pcDNA3.1(+)	Thermo Fisher Scientific	V79020
pcDNA3.1(+) expressing mouse OASIS	Saito et al. ⁹	N/A
pcDNA3.1(+) expressing human OASIS	This paper	N/A
pcDNA3.1(+) expressing human mutated OASIS (R295W)	This paper	N/A
pcDNA3.1(+) expressing mouse p53	This paper	N/A
pcDNA3.1(+) expressing mouse p21	This paper	N/A
pLenti-puro DEST (W118-1)	Addgene	17452
pLenti-puro DEST (W118-1) expressing human full-length OASIS tagged with FLAG	This paper	N/A
pLenti-puro DEST (W118-1) expressing human OASIS N-terminus tagged with FLAG	This paper	N/A
pPlatTET-gRNA2	Addgene	82559
pGL3 basic	Promega	E1751
pRL-SV40	Promega	E2231
pGL3 basic p21-Luc	Denard et al. ¹⁶	N/A
pGL3 basic Δ-CRE	This paper	N/A
pGL3 basic Δ-p53	This paper	N/A
pGEM T-easy	Promega	A1360

Software and algorithms

gRNA designer CRISPR direct	Naito et al. ³²	http://crispr.dbcls.jp
CS Analyzer 4	ATTO	2110030
Santa Cruz genome browser	Kent et al. ³³	http://genome.ucsc.edu/cgi-bin/hgGateway
DAVID Bioinformatics Resources 6.8	Huang Da et al. ³⁴ Huang Da et al. ³⁵	http://david.ncifcrf.gov
Web Multiple Experiment Viewer	Wang et al. ³⁶	https://webmev.tm4.org/about
BiQ Analyzer	Bock et al. ³⁷	http://biq-analyzer.bioinf.mpi-inf.mpg.de
ImageJ (FIJI)	Schindelin et al. ³⁸	https://imagej.nih.gov/ij/
BoxPlotR	Spitzer et al. ³⁹	http://shiny.chemgrid.org/boxplotr/

RESOURCE AVAILABILITY

Lead contact

Further information and requests for resources and reagents should be directed to and will be fulfilled by the lead contact, Atsushi Saito (saitoa@hiroshima-u.ac.jp).

Materials availability

All unique/stable reagents generated in this study are available from the [lead contact](#) with a completed Materials Transfer Agreement.

Data and code availability

- RNA-seq data have been deposited at GEO (accession number: GSE229480) and are publicly available as of the date of publication. Accession number is also listed in the [key resources table](#).
- This paper does not report original code.
- Any additional information required to reanalyze the data reported in this paper is available from the [lead contact](#) upon request.

EXPERIMENTAL MODEL AND SUBJECT DETAILS

Mice models and maintenance

8-week-old female C57BL/6J (Jackson Laboratory Japan, Yokohama, Japan) and *Oasis*^{-/-} mice (for cryoinjury to the brain cortex), and 6-week-old female BALB/c nude mice (Jackson Laboratory Japan) (for xenograft experiments) were used in this study. *Oasis*^{-/-} mice were established previously in our laboratory.⁸ In all experiments comparing *Oasis*^{+/+} and ^{-/-} primary astrocytes, osteoblasts and fibroblasts from embryonic day 18.5 (E18.5) *Oasis*^{+/+} and ^{-/-} mice, littermates generated by mating *Oasis* heterologous mice were used. C57BL/6J and *Oasis*^{-/-} mice were group-housed after weaning (2–4 mice/cage) and single housed after surgery under a 12-h light/dark cycle. Food and water were given *ad libitum*. BALB/c nude mice were housed in a pathogen-free isolation facility with a 12-h light/dark cycle and were fed rodent chow and water *ad libitum*. The experimental procedures and housing conditions for animals were approved by the Committee of Animal Experimentation, Hiroshima University (cryoinjury) and Tokushima University (xenograft experiments).

Cell culture and treatments

U251MG (JCRB Cell Bank, Ibaraki, Japan), U87MG (ATCC, Manassas, VA, USA), NP5 (JCRB Cell Bank), LN229 (ATCC), and A172 cells (JCRB Cell Bank) were maintained in Eagle's minimal essential medium (Wako, Tokyo, Japan) (U251MG and U87MG cells) or Dulbecco's modified Eagle's medium (DMEM) (Gibco, Waltham, MA, USA) (NP5, LN229, and A172 cells) supplemented with 10% fetal bovine serum (FBS) (Biosera, Kansas City, MO, USA) at 37°C in a 5% CO₂, 95% humidified air atmosphere. U251MG stably expressing human full-length OASIS tagged with FLAG (F9) or human OASIS N-terminus tagged with FLAG (N11) were cloned by drug selection using 2 µg/mL puromycin (Wako) after the transfection of pLenti-puro DEST (w118-1) (#17452) (Addgene, Watertown, MA, USA) expressing human full-length OASIS tagged with FLAG (F9) or human OASIS N-terminus tagged with FLAG (N11). Primary mouse astrocytes, osteoblasts, and fibroblasts were maintained as described previously.^{8,40} Briefly, primary astrocytes were prepared from the cerebral cortex of E18.5 *Oasis*^{+/+} and ^{-/-} littermate mice. The cortex was triturated in phosphate-buffered saline (Gibco) by mild pipetting with 1-mL pipette tips. Dissociated cells were digested with 0.05% papain (Worthington, Lakewood, NJ, USA). Isolated astrocytes were maintained in DMEM supplemented with 10% FBS. Primary osteoblasts were prepared from the calvariae of E18.5 *Oasis*^{+/+} and ^{-/-} mice. The calvariae were digested with 0.1% collagenase (Wako) and 0.2% dispase (Gibco). Isolated osteoblasts were maintained in α -MEM (Gibco) supplemented with 10% FBS. Primary fibroblasts were prepared from the skin of E18.5 *Oasis*^{+/+} and ^{-/-} mice. The skin was digested with 0.25% trypsin (Gibco). Isolated fibroblasts were maintained in DMEM supplemented with 10% FBS. Neonatal mice from which primary cells were prepared were used regardless of the sex.

To induce DNA damage by anti-cancer drugs, pretreatment with 1 µg/mL DOXO (Wako), 50 µM etoposide (Wako), or 0.5 µM 5-fluorouracil (Wako) was performed for 1 h. Cells were maintained in each culture medium for 24 h after replacing the medium three times. To induce DNA damage by irradiation, cells were exposed to 15 Gy X-rays using a Faxitron X-ray CP-160 (Faxitron, Chicago, IL, USA). The irradiated cells were maintained for 24 h. To inhibit ATR, ATM, CHK1, or CHK2 activity, cells were treated with 15 nM Ve821 (Adooq Bioscience, Irvine, CA, USA), 2.5 µM KU55933 (Adooq Bioscience), 50 nM CHIR124 (Selleck, Tokyo, Japan), or 0.5 µM CHK2in (Glix Laboratories, Hopkinton, MA, USA), respectively, for 30 h or 78 h (KU55933 for the treatment of astrocytes treated with DOXO for 72 h). The appropriate concentrations were carefully determined to check the inhibition of the phosphorylation of substrates targeted by ATM, ATR, CHK1, or CHK2 without noticeable change of cellular morphology and apoptosis because the sensitivity differs among the cell types. To induce ER stress, cells were treated with 1 µM thapsigargin (Wako) for 24 h.

METHODS DETAILS

Plasmids and siRNA

pcDNA3.1(+) (Thermo Fisher Scientific, Waltham, MA, USA) expressing mouse OASIS was constructed as described previously.⁹ pcDNA3.1(+) expressing mouse p53, mouse p21, or human OASIS was generated by PCR. pcDNA3.1(+) expressing human mutated OASIS (R295W) was constructed by inserting the cDNA of OASIS using RNA extracted from NP5 cells. pLenti-puro DEST (w118-1) (#17452) expressing human full-length OASIS and the OASIS N-terminus tagged with FLAG were generated by PCR. The cDNA sequences were as follows: mouse *Oasis*: NM_011957.2, nucleotides 66–1628; human full-length *Oasis*: NM_052854.4, nucleotides 451–2010; human *Oasis* N-terminus: NM_052854.4, nucleotides 451–1569; mouse *p53*: AB_017815.1, nucleotides 102–1274; and

mouse *p21*: AF_035683, nucleotides 53–610. Transfection of the expression vectors was performed using Avalanche-Everyday Transfection Reagent (EZ Biosystems, College Park, MD, USA) in accordance with the manufacturer's protocol. For knockdown, cells were transfected with siRNA targeting mouse *p53* (#AM16708, ID: 187426) (Thermo Fisher Scientific), human *p53* (#4390824, ID: s607) (Thermo Fisher Scientific), mouse *p21* (#4390771, ID: s63812) (Thermo Fisher Scientific), human *p21* (#4390824, ID: s415) (Thermo Fisher Scientific), human *Oasis* (#4392420, ID: s40546) (Thermo Fisher Scientific), or non-targeting siRNA (#4390843) (Thermo Fisher Scientific) by ScreenFectsiRNA (Wako). Transfected cells were incubated for 5 days for cell counting or for 48 h for all other experiments.

Epigenomic engineering

We used a validated epigenome construct containing inactive Cas9 nuclease (dCas9) and the conserved catalytic domain of TET1 (pPlatTET-gRNA2) (#82559) (Addgene).²³ In addition to GFP, this vector included GCN4 tagged with dCas9 and scFV fused to the catalytic domain of TET1 for the SUN-Tag system,⁴¹ enabling the abundant accumulation of TET1 on the targeting sequence and simultaneous expression with gRNA as an all-in-one system. For specific demethylation of the *Oasis* promoter, three types of appropriate gRNA sequences hybridizing around the CpG island of the promoter were used as queries in the gRNA designer CRISPR direct (<http://crispr.dbccls.jp>).³² These gRNAs were inserted into the validated epigenome construct. The four types of constructs expressing non-targeting (GTACGTCGGTATAACTCCTC) or each gRNA sequence hybridizing to the *Oasis* promoter (from gRNA-1: +124 bp to +146 bp, gRNA-2: +465 bp to +487 bp, gRNA-3: +940 bp to +962 bp of the *Oasis* promoter) were transfected into U251MG cells to assess the methylation status of the *Oasis* promoter by bisulfite sequencing. Among these epigenome constructs, gRNA-1 most effectively demethylated the *Oasis* promoter.

RNA isolation and RT-PCR

Total RNA was isolated from primary astrocytes using ISOGEN (Nippon Gene, Tokyo, Japan), in accordance with the manufacturer's protocol. First-strand cDNA was synthesized from 1 µg of RNA in a 20-µL reaction volume using random primers (Takara, Kusatsu, Japan) and Moloney murine leukemia virus reverse transcriptase (Invitrogen, Waltham, MA, USA). RT-PCR was performed using each specific primer set in a total volume of 20 µL containing 0.5 µM each primer, 0.2 mM dNTPs, 3 U Taq polymerase, and 10× PCR buffer (Agilent Technologies, Santa Clara, CA, USA). The primer sets used were as follows: 5'-GAACATGGAGGACTTCTC CAATG-3' (*Oasis* forward), 5'-CGGGCTCTGCTCCTGCTTCAC-3' (*Oasis* reverse); 5'-ACACGCTTGGGAATGGACAC-3' (*Xbp1* forward), 5'-CCATGGGAAGATGTTCTGGG-3' (*Xbp1* reverse); and 5'-TCCTCCCTGGAGAAGAGCTA-3' (*β-actin* forward), 5'-TCCTGCTTGCTGATCCACAT-3' (*β-actin* reverse).

Protein preparation and western blotting

Proteins were extracted from primary astrocytes, osteoblasts, and fibroblasts, and U87MG, NP5, U251MG, LN229, and A172 cells using cell lysis buffer containing 50 mM Tris-HCl (pH 7.5), 150 mM NaCl, 1% Triton X-100, and Protease Inhibitor Cocktail Set V (Wako) at 4°C. Frozen tumors were homogenized in the lysis buffer. The lysates were incubated on ice for 45 min. After centrifugation at 15,000 × g for 15 min, the protein concentrations of the supernatants were determined using a bicinchoninic acid assay kit (Thermo Fisher Scientific). Equal amounts of protein (20 µg) were subjected to sodium dodecyl sulfate-polyacrylamide gel electrophoresis. For immunoblotting, the following antibodies were used: anti-β-actin (1:100,000; Sigma-Aldrich), anti-γH2AX (1:1,000; Cell Signaling, Danvers, MA, USA), anti-p53 (1:1,000; Cell Signaling), anti-P-p53 (1:1,000; Cell Signaling), anti-cyclin B1 (1:1,000; Santa Cruz Biotechnology, Santa Cruz, CA, USA), anti-cyclin E (1:1,000; Santa Cruz Biotechnology), anti-P-ATR (1:500; Cell Signaling), anti-P-CHK1 (1:1,000; Cell Signaling), anti-cyclin D1 (1:1,000; Cell Signaling), anti-P-Y15-CDK1 (1:1,000; Cell Signaling), anti-Wee1 (1:1,000; Cell Signaling), anti-CD68 (1:1,000; Cell Signaling), and anti-p21 (1:500; Santa Cruz Biotechnology). The anti-OASIS monoclonal antibody recognizing the N-terminus of OASIS (1:1,000) was generated as described previously.⁸ The density of each band was quantified using the CS Analyzer 4 image analysis software (ATTO, Tokyo, Japan).

Immunofluorescence staining

Primary astrocytes were fixed in 4% paraformaldehyde for 1 h and permeabilized in 0.1% Triton-X 100 for 10 min. These procedures were performed at room temperature (25°C). The following antibodies were used: anti-OASIS (1:500), anti-p21 (1:500), and anti-GFP (1:500; Cell Signaling). Cells were visualized under a confocal microscope (FV1000D; Olympus, Tokyo, Japan).

Cell proliferation assay

Primary astrocytes, osteoblasts, and fibroblasts, and NP5, U251MG, and LN229 cells were seeded at 1 × 10⁵ cells/dish and cultured for 15 days. The cell number was determined using a hemocytometer (Erma, Tokyo, Japan). For the BrdU incorporation assay, cells were seeded at 5 × 10⁴ cells/well and treated with 50 µM BrdU (Sigma-Aldrich) for 6 h. After fixation by 4% paraformaldehyde (PFA), cells were treated with 1 N HCl for 15 min. To detect BrdU-positive cells, an anti-BrdU antibody (1:200; Cell Signaling) was used. After treatment with DAPI (Thermo Fisher Scientific), cells were visualized under the FV1000D confocal microscope. For flow cytometric analysis, primary astrocytes, osteoblasts, and fibroblasts, and F9, N11, U251MG, U87MG, and A172 cells (3 × 10⁷ cells) were fixed in 70% ethanol for 2 h at −30°C. After centrifugation, cell pellets were resuspended with staining buffer containing 12.5 µg/mL

propidium iodide (Sigma-Aldrich) or 1 μ g/mL DAPI (for DOXO-treated cells), 0.2 mg/mL RNase A (Nippon Gene), and 0.1% Triton X-100 for 30 min. A flow cytometer (LSRFortessa X-20; BD Biosciences, Franklin Lakes, NJ, USA) was used for analysis.

SA- β -gal staining assay

Cells were fixed in 4% PFA and stained using Senescence β -Galactosidase Staining Kit (Cell Signaling), in accordance with the manufacturer's protocol. For the staining of tumor tissues, 8- μ m frozen sections were fixed in 4% PFA and stained using Senescence β -Galactosidase Staining Kit. Cells were visualized under a microscope (BX51; Olympus). For quantitative analyses of the cultured cells, Cellular Senescence Plate Assay kit SPiDER- β -gal (Dojindo, Kumamoto, Japan) was used, in accordance with the manufacturer's protocol. Briefly, cells were lysed using the supplied lysis buffer. Lysates were placed into 96-well plates and incubated for 30 min at 37°C with SPiDER- β -gal Working Solution to react SA- β -gal with the fluorometric substrate SPiDER- β -gal. After the addition of Stop Solution, the fluorescence intensities were measured using a microplate reader, Varioskan Flash (Thermo Fisher Scientific) (Ex: 535 nm). For the quantitative analysis of tumor tissues, the images stained by SA- β -gal were captured using a microscope (BX51; Olympus) and analyzed with ImageJ.³⁸ The proportion of blue-colored area was calculated by counting the number of blue pixels relative to the total area.

TUNEL assay

U251MG cells, F9 cells, and N11 cells were fixed in 4% PFA and then permeabilized in 0.1% Triton X-100. For the staining of tumor tissues, 8- μ m frozen sections were fixed in 4% PFA. TUNEL staining was performed using DeadEnd Fluorometric TUNEL System (Promega, Madison, WI, USA), in accordance with the manufacturer's protocol. After the treatment with propidium iodide, cells and tumor tissues were visualized under a microscope (cells: FV1000D, Olympus; tumor tissues: BX51, Olympus). The treatment of cells with 200 nM staurosporine (Wako) for 24 h and the treatment of tumors with 1 U/mL DNase I (Nippon Gene) for 30 min were used as positive controls for detecting TUNEL-positive cells.

Luciferase assay

Primary astrocytes were cultured for 2 days and then transfected with 0.2 μ g of pGL3 basic reporter plasmid (Promega) carrying the firefly luciferase gene and 0.02 μ g of reference plasmid pRL-SV40 (Promega) carrying the *Renilla* luciferase gene under the control of the SV40 enhancer and promoter using ScreenFectA (Wako). Luciferase activities were measured using the Dual-Luciferase Reporter Assay System (Promega) and a GloMax Multi+ Detection System (Promega), in accordance with the manufacturer's protocol. Relative activities were defined as the ratio of firefly luciferase activity to *Renilla* luciferase activity. The *p21*-Luc reporter was kindly provided by Jin Ye (University of Texas). Δ -CRE and Δ -p53 were generated by inverse PCR using *p21*-Luc.

Bisulfite sequencing

CpG islands of *Oasis* and *p53* promoters were identified using the University of California, Santa Cruz genome browser (<http://genome.ucsc.edu/cgi-bin/hgGateway>).³³ Genomic DNA was extracted from NP5, U251MG, and LN229 cells or transplanted tumors using NucleoSpin Tissue XS (Takara). Sodium bisulfite treatment of the genomic DNA was performed using a Methylamp DNA Modification kit (Epigentek, Farmingdale, NY, USA), in accordance with the manufacturer's protocol. Regions in *Oasis* and *p53* promoters of the bisulfite-treated genomic DNA were amplified by PCR using EpiTaq HS (Takara). PCR products were cloned into a pGEM T-easy vector (Promega) and sequenced. Lollipop-style representations of five independent samples were constructed using BiQ Analyzer (<http://biq-analyzer.bioinf.mpi-inf.mpg.de>).³⁷ The conversion rates of all samples used were >95%. The primers used were as follows: 5'-GTTGTTTAAAGTTTATTTGAG-3' (*Oasis* CpG island forward), 5'-TAACACCCTAAAATTTCTAAACC-3' (*Oasis* CpG island reverse); and 5'-TAGAGTTAAAGAAATTTATTTGTG-3' (*p53* CpG island forward), 5'-CTAAACCTAAAAATAAATAC-3' (*p53* CpG island reverse).

Animal surgery

Surgical procedures were carried out under anesthesia induced by medetomidine (0.75 mg/kg), midazolam (4 mg/kg), and butorphanol (5 mg/kg). A rod prechilled with liquid nitrogen was placed in unilateral contact with the superior cranium of the left cerebral cortex of 8-week-old female *Oasis*^{+/+} or *Oasis*^{-/-} mice at 3 mm from the bregma for 1 min. The mice were sacrificed at 4 or 14 days after the surgery. Hematoxylin-eosin (HE) staining was performed using paraffin-embedded sections (6 μ m thick) by standard protocols. Immunohistochemical staining of 10- μ m-thick frozen sections using anti-GFAP (1:500; Sigma-Aldrich) and anti-CD68 (1:500) antibodies was visualized under a microscope (BX51; Olympus). The volume of the glial scar area was measured using ImageJ.

Xenograft experiment

We established an ectopic xenograft tumor model in BALB/c nude mice using U251MG cells, U251MG cells stably expressing full-length OASIS (F9), and U251MG cells stably expressing the OASIS N-terminus (N11), as described previously.⁴² A suspension of each cell type (8×10^6 cells per mouse) was mixed with an equal volume of Matrigel (Corning, Corning, NY, USA) and injected (200 μ L total volume) subcutaneously into the lower back of 6-week-old female nude mice (Jackson Laboratory Japan). The mice were housed in a pathogen-free isolation facility with a 12-h light/dark cycle and were fed rodent chow and water *ad libitum*. The tumor volume was measured with calipers for 55 days [calculated as $1/2 \times (\text{width} \times \text{length}^2)$]. Then, the animals were sacrificed

and the tumors were excised. To inject the non-targeting gRNA construct and *Oasis*-gRNA, 20 μ g of each construct (100 μ L total volume) was directly injected into the tumors using *in vivo* transfection reagent GenJet Plus (SignaGen Laboratories, Frederick, MD, USA). A portion of each tissue was fixed in 4% PFA for histological examination, and the remaining tissue sample was frozen and stored at -80°C . All animal experiments were performed in accordance with the guidelines of the animal facility at Tokushima University and approved by the Institutional Review Board. The excised tumors fixed in 4% PFA were embedded in paraffin blocks. Immunohistochemical staining of 4- μ m-thick sections of the region close to the center of the tumor using anti-Ki67 (1:500; Cell Signaling), anti-p21 (1:500), and anti-GFP (1:500) antibodies was visualized under a microscope (BX51; Olympus).

RNA sequencing

RNAs were isolated from *Oasis*^{+/+} and ^{−/−} primary astrocytes using ISOGEN in accordance with the manufacturer's protocol. The samples were evaluated using an Agilent TapeStation (Agilent Technologies) and NovaSeq 6000 (Illumina, San Diego, CA, USA) (Takara CDM Center, Kusatsu, Japan) (GSE229480). Output data were subjected to Gene Ontology and pathway analyses using DAVID Bioinformatics Resources 6.8 (<http://david.ncifcrf.gov>)^{34,35} and to the generation of a heatmap using Web Multiple Experiment Viewer (<https://webmev.tn4.org/about>).³⁶

Data collection

The correlation of gene expression with methylation was determined using Brain Lower-Grade Glioma datasets (TCGA, Firehose Legacy) on cBioportal (<https://www.cbioportal.org/>),^{28,29} and using glioblastoma multiforme, prostate cancer, colon cancer, rectal cancer, and sarcoma datasets (TCGA, legacy TCGA) on UCSC Xena Browser (UCSC Xena, <https://xenabrowser.net>).³⁰ The correlation of gene expression with methylation in glioblastoma cell lines was determined using Cancer Cell Line Encyclopedia (<https://sites.broadinstitute.org/ccle/>).³¹

QUANTIFICATION AND STATISTICAL ANALYSIS

Statistical comparisons were made using unpaired Student's *t*-test (between two samples) and one-way ANOVA followed by Tukey's *post hoc* test (among multiple samples). To construct boxplots, the web tool BoxPlotR (<http://shiny.chemgrid.org/boxplotr/>)³⁹ was used. Differences were considered statistically significant at $p < 0.05$. *p*-values of less than 0.05 and 0.01 are indicated as * and **, respectively. We confirmed the validity of the biological replicates and enhanced the reliability of the data by repeatedly performing independent experiments using more than three independent samples.